Measurement of Panel Reflection Using Acoustical Scale Modeling Techniques*

JOSE C. ORTEGA

Paul S. Veneklasen and Associates, Santa Monica, CA 90404, USA

The importance of early reflected sound from sidewall and ceiling reflecting panels in auditoriums and spaces used for musical presentation has been recognized for some time. Experience teaches that the size, shape, and orientation of the panels affect their reflecting characteristics. Results of ongoing studies using scale modeling techniques are presented. The measured reflection transfer function is given for several types of reflecting panels. Transfer functions measured in the shadow zone of a reflecting panel exhibit interference characteristics. The nonuniformity of the transfer functions is shown to be due to out-of-phase waves diffracted from the panel edges.

0 INTRODUCTION

The reflecting characteristics for panels used to produce early lateral reflections can influence the spatial perception in auditoriums. It is generally agreed that the size, shape, and orientation of reflecting panels affect their reflecting characteristics. Quantitative data relating size, shape, and orientation, while not totally lacking, are not abundant. This paper presents the results of a modest effort to obtain the reflecting characteristics of a number of simple panels using acoustical scale modeling techniques.

The measurement facility, procedure, and instrumentation used are presented in Secs. 1–3. The measured reflection transfer functions are presented in Sec. 4, where panel width, panel type, and measurement angle of the reflected sound are compared. A general discussion of the results is presented in Sec. 5 and a summary in Sec. 6.

1 MEASUREMENT APPARATUS AND FACILITY

Fig. 1 shows the anechoic space used for all results reported here. The inside dimensions are 1.4 m wide by 1.1 m deep by 0.96 m high. The walls and ceiling of the chamber are composites of low-density and medium-density fiberglass materials covered on the inside surface with a quilted cheese cloth. The floor of the chamber is made of 0.05-m-thick medium-density fiberglass panels covered with a hardware cloth. The space has been found to obey the inverse square law for frequencies in excess of about 1000 Hz. Fig. 1 also shows a typical arrangement for measuring reflections from a 0.1-m-wide by 0.61-m-high flat panel. The spark probe is located to the left of the panel and the microphone to the right. The microphone is oriented so that regardless of its location, all acoustic signals from the spark source or from the panel arrive at the microphone diaphragm at grazing incidence. This procedure eliminates frequency response variations of the microphone, which would then have to be accounted for in subsequent data reduction.

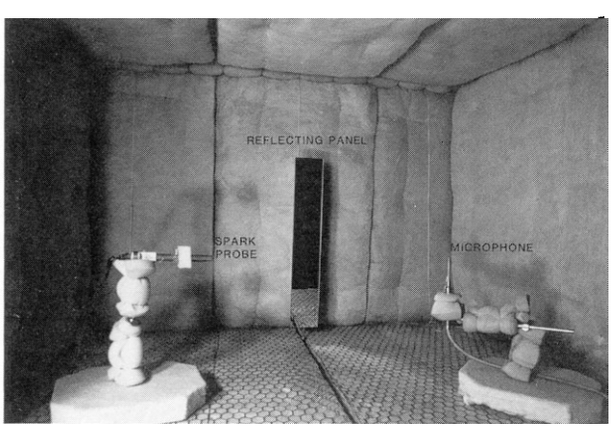

Fig. 1. Anechoic chamber and typical experimental setup.

* Presented at the 89th Convention of the Audio Engineering Society, Los Angeles, 1990 September 21–25; revised 1991 January 22 and May 24.

The sound source used in the measurements was an electric spark. Two 2.5-mm-diameter brass rods are used to hold small-diameter tungsten wires. The ends of the tungsten wires are separated to form the spark gap. The circuit used to generate the spark maintains a potential in excess of 1100 V across the gap prior to firing. A triggering circuit in conjunction with a thyratron is used to initiate the spark. The generated spark produces an acoustic waveform that approximates an N wave with a duration of about 18 μs. Details of the spark probe have been presented by Veneklasen [1].

Three types of panels have been studied: flat, curved (with the convex surface utilized), and segmented. All flat panels were made from 3.2-mm-thick mirrored glass. All panels were 0.61 m long. Four flat panels were used. The widths of the flat panels were 0.025, 0.05, 0.10, and 0.15 m. The curved panel was made of a sheet of flat aluminum fastened to a series of curved ribs similar to the way an airfoil is assembled. The width of the curved panel was 0.15 m. The radius of curvature of the curved panel was 0.24 m. The segmented panel was flat and composed of 12 small mirrored glass panels attached to a steel rod framework. The diameter of the steel rods, which connected the individual small glass panels to form an array, was 0.003 m and would not be expected to contribute to the reflected pulse. The individual small panels were 0.06 m wide by 0.08 m high and were separated from each other by a distance of 0.025 m. The nominal outside dimensions of the segmented panel were 0.15 m wide by 0.61 m high, which was equal in size to the curved panel and the largest of the flat panels.

2 MEASUREMENT PROCEDURE

A description of the method of measurement is best facilitated by referring to Fig. 2. The sound source on the left was located 0.61 m from the reflecting panel shown at top center. The angle of sound incidence on the panel was 30° and was held constant for all measurements reported here. This incident angle and the measurement angles, between 0 and 60°, are typical of those used in concert-hall design to provide early lateral reflections. The location and orientation of the reflecting panel were also held constant for all measurements. The measurement microphone was located on the arc of a circle with its center at the panel center. The location of the microphone on this arc varied depending on the objectives of the experiment. Note that at a reflecting angle of 30° the microphone is located at the center of the specular reflection zone. For the 0.15-m-wide panel shown the specular reflection limits subtend a total angle of about 26°. For a panel of a lesser width specular reflection limits are of course narrower.

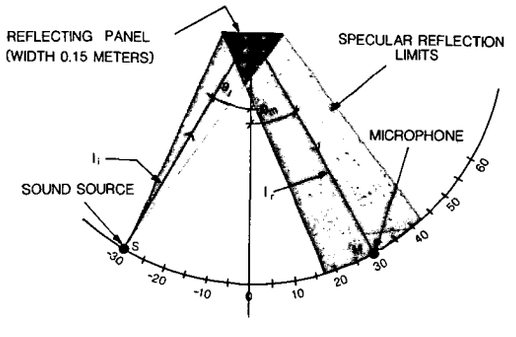

Fig. 2. Plan view of measurement geometry. θ_i—angle of incidence; θ_m—angle of measurement; I_r—reflection path length 0.61 m; I_i—incident path length 0.61 m.

The sound source used in these experiments is a point source and is small compared to the wavelengths over the frequency range of interest. The distances between the sound source and the reflecting panel and between the reflecting panel and the point of measurement are large compared to the wavelength. Hence these measurements can be considered to be made in the far field of source and reflecting panel. The measurement procedure was as follows:

1) With the reflecting panel removed, the microphone was placed at the location of the center of the panel. Three separate acoustic pulses were captured using the transient capture mode of the analyzer. The three pressure–time histories were then transferred and stored in digital form on the hard disk of the computer. These pulses represent the incident acoustic wave on the panels.

The location of the microphone for this measurement was prompted by the fact that the acoustic radiation of the spark is not perfectly spherical, that is, small variations in pulse shape and, hence, spectrum were noted at different angles around the spark source. To avoid having to account for these small variations, it was felt that the incident acoustic pulse should be that which is actually incident on the panel. The size of the anechoic chamber did not permit placing the microphone at a distance equal to the total path length of the reflected pulse.

2) Next the microphone was moved to one of the locations on the arc and a panel placed, as shown in the figure. Again, three pressure–time histories were captured and stored in the computer. In this case the captured traces exhibit first a direct pulse, since its path length is shorter than the path length for the reflected pulse, and at a later time (1–2 ms) the reflected pulse. The input attenuator of the analyzer is set so that the amplitude of the reflected pulse is maximized in order to maximize the signal for this portion of the pressure–time trace. The three reflected pulses represent the reflected acoustic wave from the panel.

3) The computer and the analyzer are now used to obtain averaged spectra of the incident and reflected waves. Prior to obtaining the spectra, the pressure–time traces are windowed so as to eliminate noise and small signals that are not associated with the incident and reflected pulses. The width of the windows used was chosen after close examination of the pressure–time traces. This procedure has been found to have no effect on the spectrum of the pulses in the frequency range of interest, which for these experiments is from

5 kHz to 100 kHz, and has also been found to improve the signal-to-noise ratio. An example of a reflected pulse before and after windowing is shown in Fig. 3.

The reason for the "noisiness" of the trace before windowing is due to the greatly increased vertical gain of the analyzer, which is required in order to see the reflected wave. In the case shown, the reflected wave is very much smaller than the direct wave which is not shown in the figure.

4) Finally, the analyzer and the computer are used to obtain the reflection transfer function of the panel, which is defined here as the ratio of the reflected spectrum to the incident spectrum. Adjustments to the reflected spectrum are made prior to obtaining the transfer function. The adjustments account for the added absorption and inverse square loss suffered by the reflected wave due to its longer path length. For the geometry used in these experiments, the inverse square loss adjustment is +6 dB. The adjustment for air absorption is a function of frequency, temperature, and relative humidity. The air absorption adjustment was made using the procedure presented in ANSI S1.26-1978 [2].

3 INSTRUMENTATION

The instrumentation used to measure the reflection transfer function of the panels is shown in Fig. 4. This instrumentation is similar to that used in earlier studies with the addition of the computer and the digital plotter. Earlier studies used a ¼-in (6-mm) microphone. The present study utilized a ⅛-in (3-mm) microphone. The high-pass filter is used to exclude extraneous noise at frequencies below the range of interest. The FFT analyzer shown captures in digital-format 1024 data points of the pressure–time traces sensed by the microphone. These data are then transferred to the computer for permanent storage. The frequency response of the system is shown in Fig. 5.

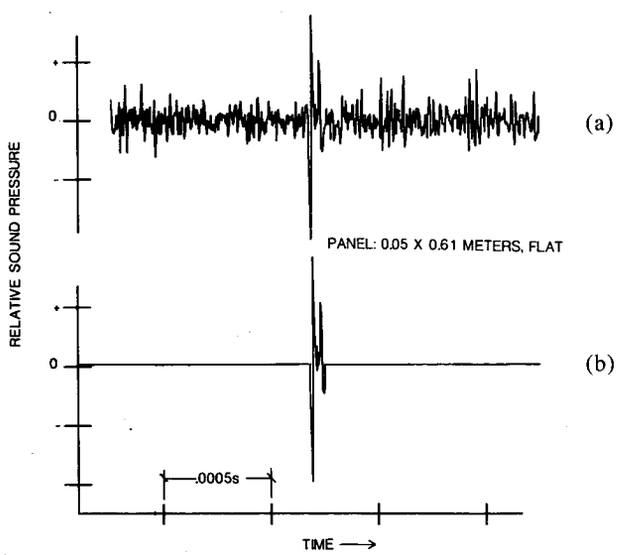

Fig. 3. Reflected pressure–time trace $\theta_m = 10°$. (a) Before windowing. (b) After windowing.

4 MEASUREMENT RESULTS

4.1 Incident and Reflected Waves

Fig. 6 presents a typical result showing the incident wave and the reflected wave from a flat panel. The microphone location for the measurement was at 30° (see Fig. 2), which corresponds to the center of the specular reflection zone. The measured spectrum of the incident pulse is shown in Fig. 7. The spectrum of the incident pulse, which has a duration of about 18 μs and which approximates an *N* wave, is expected to have a maximum near 45 kHz. The rolloff of the spectrum shown is a characteristic of the pulse described; however, a portion of this rolloff above 70 kHz is due to the response of the microphone, which for reasons discussed earlier is used with the incident sound wave grazing the microphone diaphragm.

4.2 Diffracted Waves

Locating the measurement microphone out of the specular reflection zone or in the shadow zone produces

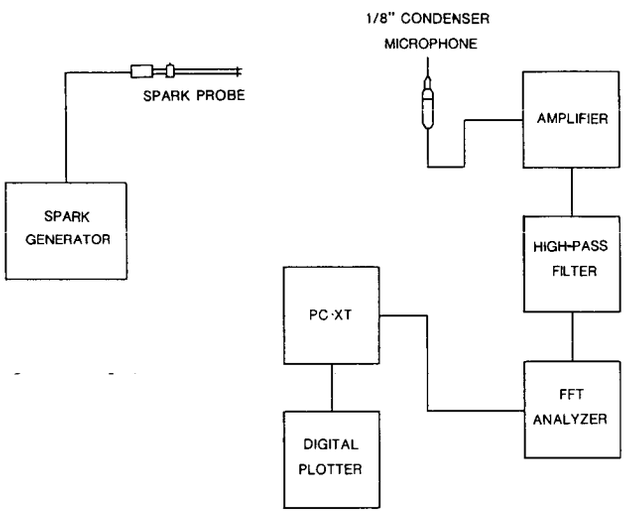

Fig. 4. Instrumentation diagram.

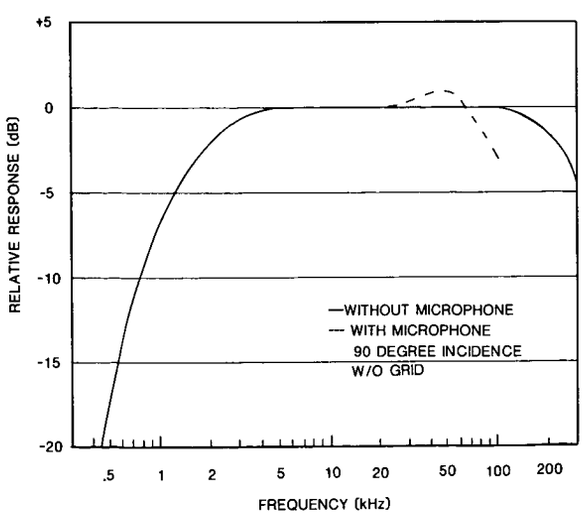

Fig. 5. Measurement system frequency response.

some interesting results. The first result is that there are always two waves. These two waves are associated with diffracted energy from the panel edges. In optical and acoustical work they are generally referred to as edge waves. The second point of interest is that the two waves are 180° out of phase with each other. An example of this is shown in Fig. 8 using the 0.05-m-wide flat panel with the microphone at 45°. The separation between the edge waves is 34.4 μs, which will be shown later to correspond to expected travel time difference between the panel edges. The out-of-phase relationship is explained from optical theory and is discussed in a later section.

4.3 Transfer Functions

4.3.1 Panel Width

The measured transfer functions for the four flat panels with different widths are presented in Fig. 9. The angle of incidence on the panel was 30°. The microphone was located at an angle of 30°. Recall that this microphone location is the center of the specular reflection zone.

The results shown here agree qualitatively with theory, that is, for the two larger panels the transfer function is near 0 dB. The term "larger" used here is in reference to the wavelength. For example, at 10 kHz the wavelength is about 0.04 m. At this frequency, therefore, the 0.1-m and 0.15-m-wide panels are several wavelengths wide. The oscillations above and below 0 dB for the large panels are also predicted by theory. When the panel width is not large relative to a wavelength, then the transfer function is expected to decrease. The 0.025- and 0.05-m panels show this expected characteristic.

4.3.2 Panel Type

Fig. 10 compares the measured transfer functions for three different types of panels of the same outside dimensions. The angle of incidence and the measurement angle were held constant at 30°. The variable here is the panel type. Again, the flat panel oscillates near 0 dB. The curved panel, on the other hand, has a lower amplitude transfer function. However, it exhibits a more uniform frequency response. A calculation of

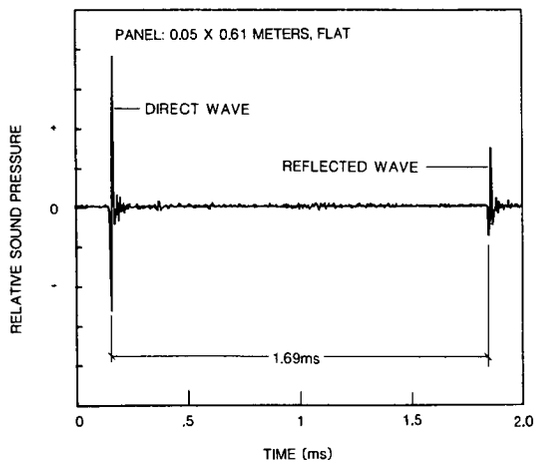

Fig. 6. Typical pressure–time trace of direct and reflected waves. θ_i, θ_m = 30°.

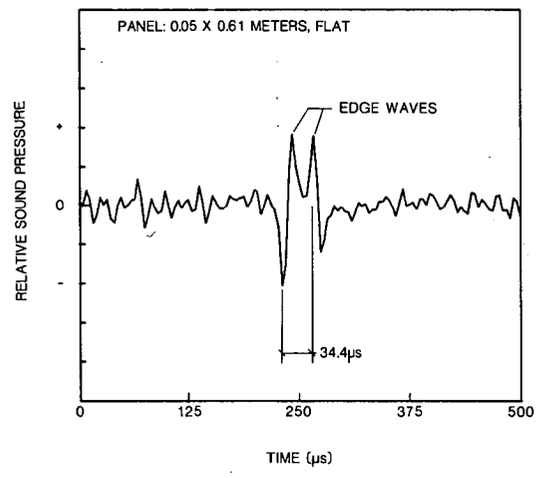

Fig. 8. Edge waves measured in shadow zone of a reflecting panel. θ_i = 30°; θ_m = 45°.

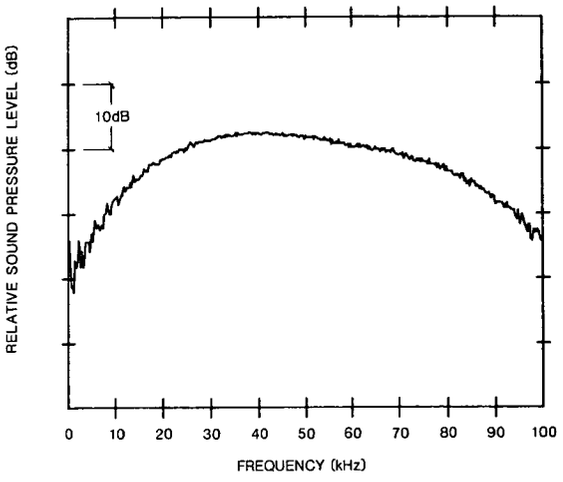

Fig. 7. Measured spark source spectrum. Measurement distance 0.61 m.

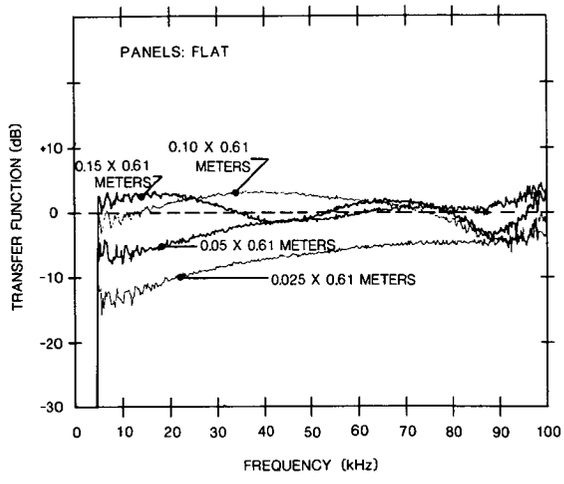

Fig. 9. Transfer function versus panel width. θ_i, θ_m = 30°.

the expected reduction in the transfer function of the curved panel versus a flat panel of equal width, based on the total subtended angles of the specular reflection limits, indicates that the reduction should be about 6 dB for the two panels shown. The actual measured value is on the average about 7 dB.

The segmented panel exhibits a very nonuniform response of diminished amplitude over most of the frequency range measured. The numerous edges associated with this panel construction are believed to contribute to the nonuniform response. The diminished amplitude is due primarily to the relatively small size of the reflecting segments of the panel. It should be stated here that the location of the microphone was such that no portion of the segmented panel produced a specular reflection to the microphone. On the other hand, edge waves are numerous for this type of panel, and, as will be shown later, edge waves contribute to nonuniform transfer functions.

4.3.3 Measurement Angle

Figs. 11–13 present the measured transfer function when the location of the measurement microphone on the arc of constant radius is the variable. The results for the 0.15-m-wide flat panel are shown on Fig. 11. The 20° and 30° locations are within the specular reflection zone for this panel. The 10° location is in the shadow zone, and the change in transfer function is dramatic. Fig. 12 presents results for the 0.15-m-wide curved panel. The same three angles as used in Fig. 11 for the flat panel are shown here. For this panel all three angles are within the specular reflection limits. In fact, for this panel data measured over a 60° range show results very similar to those shown in Fig. 12. Due to the curvature, all of the points with this 60° range are within the specular reflection limits of the panel.

Fig. 13 shows the measured transfer function versus measurement angle for the 0.05-m-wide flat panel. In this case the 20° and 10° curves are outside the specular reflection limits, and again a dramatic change in response is exhibited.

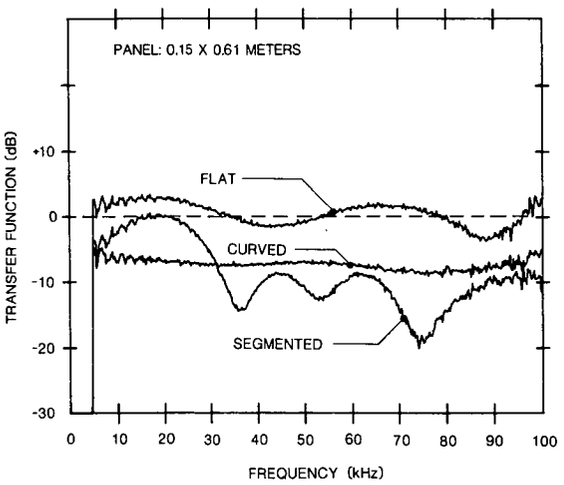

Fig. 10. Transfer function versus panel type. θ_i, θ_m = 30°.

5 DISCUSSION

5.1 Fresnel Zone Effects in Specular Reflection Zone

The measured transfer functions in the specular reflection zone for large panels (that is, large relative to wavelength) exhibit oscillations about 0 dB. These oscillations are explained qualitatively by Fresnel half-period zones described in Jenkins and White [3]. Any finite-sized reflecting panel intercepts a portion of an incident wavefront, which contains at any given frequency a number of half-period Fresnel zones. For any particular observation point in the specular reflection region, a half-period Fresnel zone, due to the method used to define the zones, contributes energy that is 180° out of phase with its two adjacent zones. The resulting amplitude at a given location in the specular reflection zone depends on the number of intercepted Fresnel zones. The area of the Fresnel zones are a function of the distance between sound source and measurement microphone to the reflecting panel and

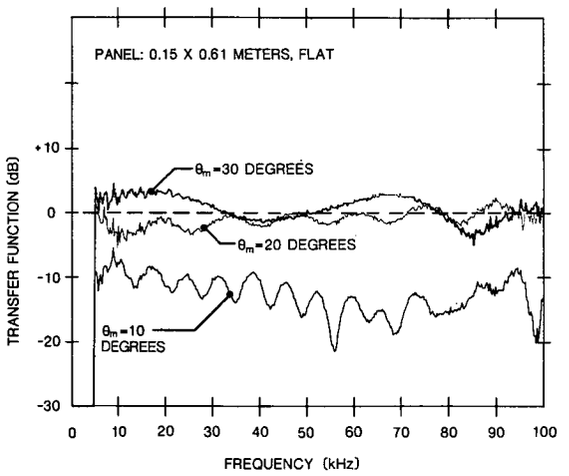

Fig. 11. Transfer function versus measurement angle. θ_i = 30°.

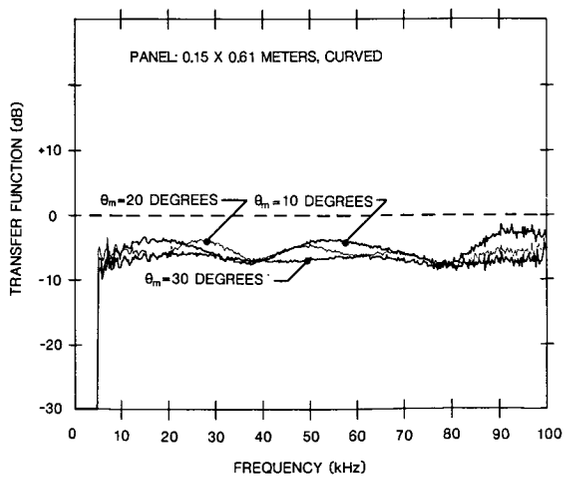

Fig. 12. Transfer function versus measurement angle. θ_i = 30°.

also of frequency. The oscillations of the transfer function about 0 dB correspond to the changing number of zones intercepted by the reflecting panel when frequency is varied.

5.2 Edge Wave Effects in the Shadow Zone

A discussion of the edge waves noted earlier is facilitated by reference to diffraction theory found in optical textbooks. In general, diffraction theory in optics is developed utilizing slits and apertures. The experiments presented in this paper utilized reflecting surfaces instead of apertures. It turns out, however, that the experiments performed using reflecting panels have a corresponding counterpart in terms of apertures. The concept presented here is borrowed from Rayleigh [4]. Fig. 14(a) illustrates the experimental scheme used for this paper. Sound waves from source S_0 are reflected from the panel to the microphone at M. Diffracted waves are generated at edges A and B of the panel. The image of source S_0 is S_i, located as shown. Rayleigh shows that if the sound source is moved to the location of the image source S_i and if the rectangular reflecting panel is replaced by a rectangular aperture of identical dimensions, and if further, an infinite baffle is placed around the aperture, then experiments performed in the modified condition produce results that are identical to those of the original scheme. The modified scheme, which is the complement of the measurement scheme used in this work, is shown in Fig. 14(b) and is typical of the situation utilized in optical experiments. Hence the results presented here can be compared or discussed using optical theory. This result is not surprising. Interchanging concepts in optics and acoustics is not a novel approach.

Returning to Fig. 14(b), theory shows that edge waves radiated into the shadow zone are generated at edges A and B. The edge wave radiated into zone A from edge A is referred to as an inflected wave, while that from edge B is referred to as a deflected wave. Similarly, in zone B the edge wave from edge B is an inflected wave and the edge wave from edge A is a deflected wave. It turns out that the two edge waves radiating into the shadow zones are out of phase with each other by 180°. This stems from the result that the inflected wave suffers a retardation of one-eighth of a wavelength with respect to the undisturbed wave (that is, the wave in the specular reflection zone) and the deflected wave suffers a retardation of five-eighths of a wavelength. This difference translates to a one-half-wavelength retardation of the deflected wave with respect to the inflected wave, or a 180° phase difference. A clear presentation of this phenomenon is given by Meyer [5]. In terms of arrival sequence into the shadow zone, the geometry of Fig. 14(b) shows that the inflected edge wave will always arrive earlier than the deflected wave.

In order to check the validity of this concept, measurement of the difference in arrival time between the two edge waves was performed and compared to the expected difference based on the geometry of the measurement setup (see Fig. 2). An example of edge waves produced by two different-width panels at the same measurement angle is shown in Fig. 15. The computer was used to expand the horizontal time scale so that time differences could be measured from the plotted data. A comparison between the measured time differences between the two edge waves and the calculated values for two flat panels is shown in Fig. 16. The relations used to calculate the transit time differences between the two edge waves are presented in the Appendix. The lack of measured time differences in Fig. 16 in the specular reflection zone areas does not imply that edge waves are not present, only that the direct wave whose amplitude is so much greater does not allow them to be detected.

The preceding discussion and results can be used to

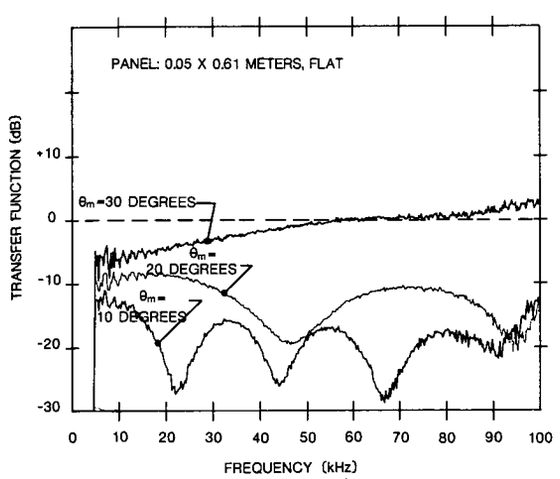

Fig. 13. Transfer function versus measurement angle. θ_i = 30°.

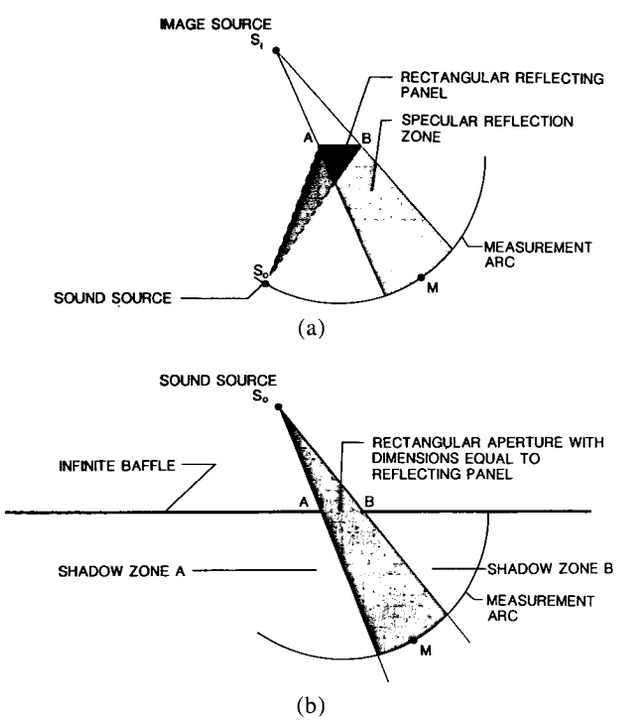

Fig. 14. Complementary experimental setups.

explain the transfer function measured when the measurement microphone is in the shadow zone of the reflecting panel. Fig. 17 presents transfer functions measured using the 0.05-m-wide flat panel with the microphone in the shadow zone. The characteristics of both curves indicate that destructive interference between the two edge waves is present. A simple calculation confirms this point. The edge wave arrival time difference for the 10° curve corresponds to a path-length difference of 1.26×10^{-3} m. This path-length difference corresponds to a wavelength at about 22.7 kHz. The initial point of destructive interference shown for the 10° curve is very close to the calculated value, and subsequent points of destructive interference are located as expected. A similar calculation for the 20° curve shows that the path-length difference corresponds to a wavelength at about 45.5 kHz. The measured data exhibit destructive interference effects at 46.7 and 94.5 kHz, which are 47.8 kHz apart. Hence the two edge waves, which are always present in the shadow zone of the reflecting panel, produce transfer functions that exhibit destructive interference.

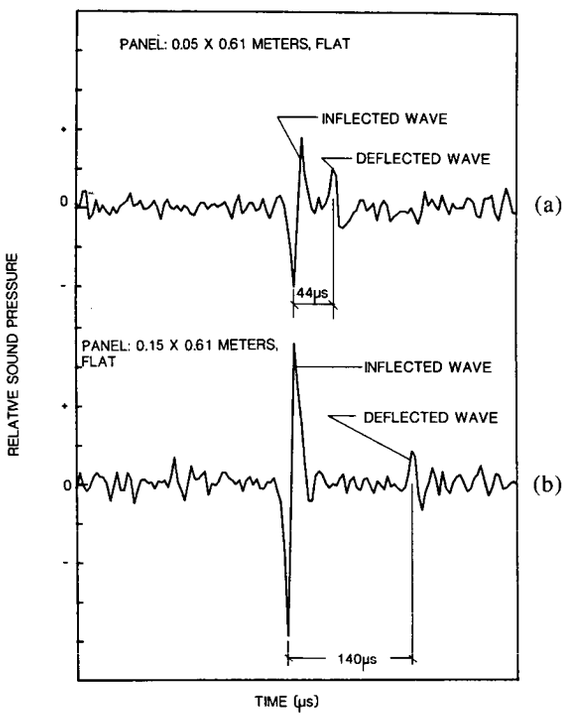

Fig. 15. Inflected and deflected edge waves measured in shadow zone of a reflecting panel. $\theta_i = 30°$; $\theta_m = 10°$.

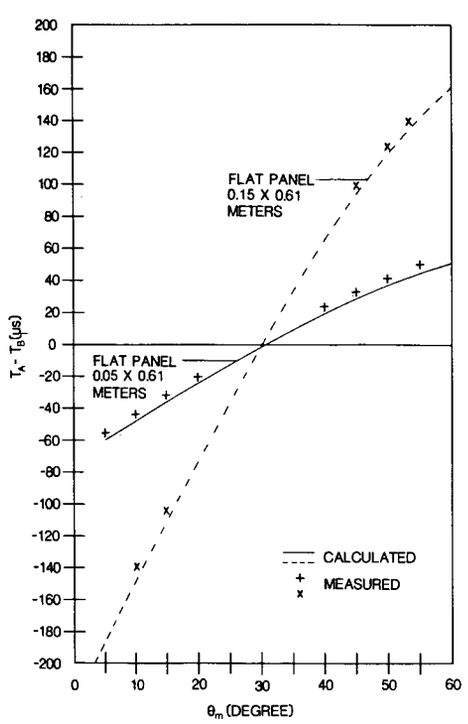

Fig. 16. Measured and calculated edge wave transit time differences.

The practical implication of a nonuniform transfer function is that the reflected wave is distorted relative to the incident wave. In an auditorium where sidewall reflecting panels are utilized this means that early reflected sound would be distorted relative to the direct sound from the stage to an observer in the audience. Other studies have shown that subjects prefer early reflected sound which faithfully reproduces the direct sound [6], [7]. Hence, a nonuniform transfer function can result in coloration of the reflected sound, which is judged to be less desirable than reflected sound with full uniform bandwidth.

6 SUMMARY

The results of the experiments reported here can be summarized as follows.

1) Wide-band and relatively uniform spectral reflections are achieved only when a flat reflecting panel is large compared to the longest wavelength of interest. Furthermore, these wide-band and uniform spectral reflections are achieved even for large flat panels only when the observation point is located within the specular reflection zone of the panel.

2) A large curved panel with convex surface exhibits

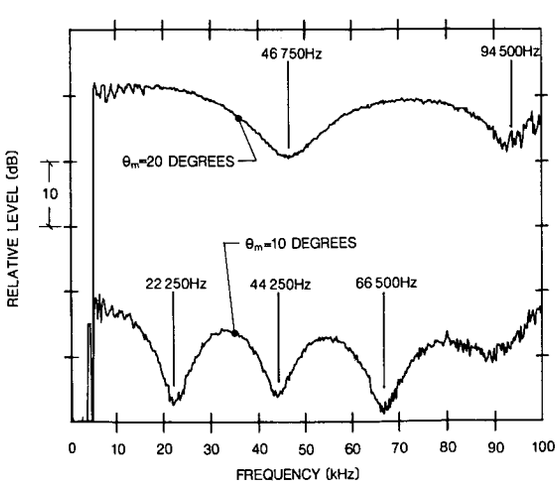

Fig. 17. Transfer functions exhibiting edge wave interference effects.

a transfer function which has an amplitude that is less than that of a flat panel of similar size. However, this deficiency is balanced by a greatly increased specular reflection zone over which relatively smooth wide-band reflections are exhibited.

3) The segmented panel measured resulted in a transfer function that exhibited a lower amplitude and a nonuniform frequency characteristic. This nonuniformity is the result of numerous edge effects similar to those discussed in this paper.

4) Measurement locations which are outside the specular reflection limits of reflecting panels exhibit transfer functions that are small in amplitude and nonuniform with frequency due to interference effects.

5) Panels used in auditoriums to provide early lateral reflections should be designed to provide uniform reflection characteristics of full bandwidth in order to avoid coloration of the reflected sound.

7 ACKNOWLEDGMENT

This work was supported by the Paul S. Veneklasen Research Foundation. The author wishes to thank several of his colleagues at Paul S. Veneklasen and Associates for their encouragement and helpful discussions. These include Paul Veneklasen, Jerry Christoff, Gary Mange, Hooshang Khosrovani, and Neil Shaw. Gary Mange developed the computer program utilized in the experiments.

8 REFERENCES

[1] P. S. Veneklasen, "Model Techniques in Architectural Acoustics," *J. Acoust. Soc. Am.*, vol. 47, pp. 419–423 (1980 Feb.).

[2] ANSI S1.26-1978, "Method for the Calculation of the Absorption of Sound in the Atmosphere, American National Standards Institute, New York (1978).

[3] F. A. Jenkins and A. E. White, *Fundamentals of Optics*, 2d ed. (McGraw-Hill, New York, 1950), pp. 347–375.

[4] J. W. Strutt, Baron Rayleigh, *The Theory of Sound*, 2d ed., vol. 2 (Dover, New York, 1945), pp. 118–122.

[5] C. F. Meyer, *The Diffraction of Light, X-Rays, and Material Particles*, 2d rev. ed. (J. W. Edwards, Ann Arbor, MI, 1949), pp. 222–233.

[6] J. Blauert and W. Lindeman, "Explorative Studies on Auditory Spaciousness," in *Proc. Vancouver Symp. on Acoustics and Theatre Planning for the Performing Arts* (Vancouver, Canada, 1986 Aug.).

[7] Y. Ando, *Concert Hall Acoustics*, Springer Series on Electrophysics, no. 17 (1985), pp. 56–59.

APPENDIX
EDGE WAVE TRANSIT TIME DIFFERENCES

The relationships used to calculate edge wave transit time differences are derived from the geometry shown in Fig. 18. The transit time from source S to receiver M via edge A is T_A. The transit time from source to receiver via edge B is T_B. the transit time difference is defined here as

$$T_A - T_B = \frac{L_2 + L_3}{c} - \frac{L_4 + L_5}{c} \tag{1}$$

where c is the velocity of sound. From Fig. 18 we have

$$L_2^2 = y^2 + x^2 \tag{2}$$

but

$$y^2 = L_1^2 \cos^2 \theta_i \tag{3}$$

$$x^2 = \left(L_i \sin \theta_i - \frac{d}{2}\right)^2 . \tag{4}$$

Substituting Eqs. (3) and (4) into Eq. (2) and simplifying leads to

$$L_2 = \left(L_1^2 - L_1 d \sin \theta_i + \frac{d^2}{4}\right)^{1/2} . \tag{5}$$

Similar derivations for L_3, L_4 and L_5 lead to the following equations:

$$L_3 = \left(L_1^2 + L_1 d \sin \theta_m + \frac{d^2}{4}\right)^{1/2} \tag{6}$$

$$L_4 = \left(L_1^2 + L_1 d \sin \theta_i + \frac{d^2}{4}\right)^{1/2} \tag{7}$$

$$L_5 = \left(L_1^2 - L_1 d \sin \theta_m + \frac{d^2}{4}\right)^{1/2} . \tag{8}$$

In deriving Eqs. (6) and (8) use is made of the identity

$$\cos \beta = \cos (90° - \theta_m) = \sin \theta_m . \tag{9}$$

The equations for L_2, L_3, L_4, and L_5 are used in Eq. (1) to obtain the values for the transit time differences presented in this paper.

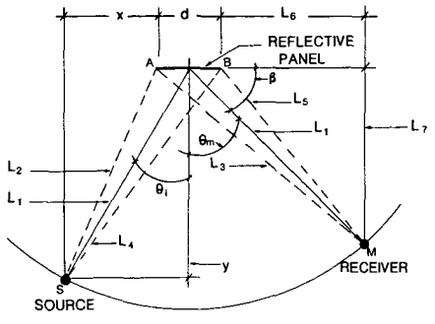

Fig. 18. Transit time geometry. θ_i—angle of incidence; θ_m— angle of measurement.

THE AUTHOR

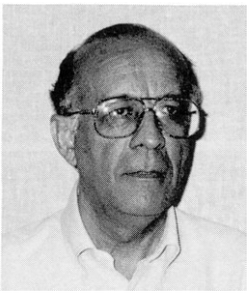

Jose C. Ortega received a B.S. degree in physics from the University of California, at Los Angeles (UCLA), in 1957. Graduate work in physics with emphasis in acoustics led to an M.S. degree in 1961 from UCLA. He began his professional career in 1956 at Paul S. Veneklasen and Associates and its affiliate Western Electro-Acoustic Laboratory and that association continues. His professional work has included microphone design and calibration, jet aircraft noise suppression, environmental noise studies, development of instrumentation and measurement methods related to acoustical scale models, managing an acoustical laboratory for testing of commercial products, and the design and evaluation of auditoria, television, and recording studios. Mr. Ortega is currently a principal associate at Paul A. Veneklasen and Associates and vice president of Western Electro-Acoustic Laboratory.